Performance Evaluation of the Aventech AIMMS20AQ Aircraft Wind System

David J. Delene and Christopher Kruse

Abstract

We compare two independent calibration methods for the commercially available Aircraft Integrated Meteorological Measurement System (AIMMS) airborne wind measurement system. The first is Aventech's standard calibration method implemented using the company's proprietary software. The second is the University of North Dakota (UND) calibration method used on the Citation Research Aircraft for several decades and implemented as part of the Airborne Data Processing and Analysis (ADPAA) open source software package. The performance of both methods is evaluated using the mean and variance of wind measurements obtained during validation flight maneuvers designed to test how extremes in aircraft motion affect each wind vector component. The two methods produced similar statistical distributions of the wind vectors. Neither method completely removed the effects of the aircraft maneuvers from the wind solution, with both methods resulting in an increase in standard deviation of 0.1 m s^{-1} in the vertical wind solution when porpoise maneuvers were performed. However, the increase in vertical wind component variance is less when using the manufacturer's calibration method. There is a dependence of up to 3 hPa in the static pressure measurements due to airflow angles and air speed effects that result from the gust probe being located on the aircraft's wing which is not accounted for in either method. The favorable comparison between the two wind solution methods and small increases in wind components during validation maneuvers indicates that both methods obtain scientifically useful atmospheric winds measurements when deploying the AIMMS probe on research aircraft. However, the implementation of the UND method in the ADPAA open source package allow scientist to improve the method further without having to repeat the software development work. Furthermore, having open source software allows for the repeatability of scientific work since the code can be modified to work on any gust probe system as demonstrated by its implementation on the UND Citation Research Aircraft.

Introduction

Vertical wind velocity is an important parameter for cloud physics research (Snider et al., 2003) and boundary layer flux measurements (Lenschow 1979, Bange et. al. 2002, Karl et. al. 2009). Aircraft-based wind measurements are often conducted since the sampling location can be targeted and many additional parameters can be measured simultaneously. This allows for several types of flux measurements to be made and for the relationship between aerosol and cloud droplets to be studied. Delene et al., 2011 found a relationship between Cloud Condensation Nuclei (CCN) and cloud droplet concentrations in cumulus clouds; however, the relationship accounted for less than 50% of the variance. Variations in supersaturation are probably responsible for much of the remaining variance. Accounting for this remaining variance is not possible using direct humidity measurement to determine supersaturation. Airborne temperature, dew point temperature and absolution humidity measurements do not have the accuracy necessary. However, updraft velocity (vertical wind velocity) near cloud base can be measured and used to infer the maximum supersaturation experienced by a rising air parcel. Hence, aircraft-based vertical wind measurements are critical when relating the CCN supersaturation spectrum to the measured cloud droplet spectrum.

The wind velocity is the vector sum of the velocity of the aircraft with respect to the ground and the velocity of the air with respect to the aircraft (Lenchow 1986). The Air velocity vector with respect to the aircraft is commonly measured either by using vanes that point into the flow direction (Lenschow 1972), or by using pressure ports on a mounted hemispherical gust probe (Crawford and Dobosy 1992) or aircraft radome (Kalogiros 2002). Gust probes have been preferred instead of vanes because of the high accuracy and sampling rates of current pressure transducers. Also, a hemispherical probe distorts the airflow less than a wind vane boom, providing more representative measurements of the unperturbed atmosphere. The optimal location of a gust probe would be on the aircraft where flow is minimally distorted; however, positioning the gust probe in this optimal location can be costly or impossible due to existing instrumentation, airframe characteristics, and safety considerations.

The aircraft velocity relative to the ground is often found using an Inertial Navigation System (INS) that is coupled to a Global Positioning Systems (GPS). The INS is usually mounted near the center of gravity (CG) of the aircraft. A coupled INS/GPS system has the high accuracy of an INS; however, the GPS prevents INS errors from accumulating with time. The INS is also used to determine instantaneous attitude along with rate of change of attitude information. In many state-of-the-art systems, a differential GPS is used instead of a single antenna system. A differential GPS utilizes a minimum of two GPS antennas that are usually positioned on the wings to improve the quality of the position information.

Recent studies on small (Wood 1997, Beswick 2008) and large (Khelif 1999, Kalogiros and Wang 2002) aircraft have focused on the calibration and evaluation of three dimensional wind measurements. While some research has focused on vertical wind, most of the measurements were conducted in an environment where the wind field was uniform and not turbulent. The Lenschow (1986) equations for the east, north, and upward wind components are used in most publications dealing with aircraft-based wind measurements. These equations include effects due to the INS and gust probe not being at the same location; however, it is assumed that the gust probe is along the longitudinal axis of the aircraft. The Beswick (2008) and Van Den Kroonenberg (2008) studies assumed that gust probe velocities measured due to rotation of the aircraft are negligible, whereas in other studies (Tjernstrom and Friehe 1991, Khelif 1999, Kalogiros 2002) the pressure measurements are taken on the longitudinal axis of the aircraft and the Lenschow equations are valid. During normal flight conditions in non-turbulent air, the effects of aircraft rotation are not important, but the effects of aircraft rotation become increasingly important where significant turbulence (and therefore rapid attitude corrections) is present (thunderstorms, boundary layer, etc). Hence, in these cases, modified equations for gust probe measurements along the wing of an aircraft are necessary.

1. Airborne Measurements

This paper focuses on wind measurements from the commercially available Aircraft Integrated Meteorological Measurement System (AIMMS, Aventech Research Inc.) and provides a comparison between two calibration methods which use different aircraft maneuvers and calibration constraints. The AIMMS probe was flown (16 flights between 15 April and 14 March 2009) on a specially instrumented Beech King Air B200 (Tail Number N825ST) during the Spring 2009 Saudi Arabia Rainfall Augmentation project (University of North Dakota, 2009). The research aircraft was equipped to measure atmospheric state parameters and also equipped with aerosol and cloud physics instrumentation (Kucera et al., 2010). The research objective involved conducting boundary layer and in-situ cloud measurements to better understand the aerosol and cloud characteristics and precipitation formation processes in central Saudi Arabia, for which vertical velocity is an important parameter (Snider et al., 2003).

As shown in Fig. 1, the GPS antennas were located just outboard from each nacelle (6.613 m separation distance), the Air Data Probe was located away (5.918 m) from the inertial measurement unit (IMU) on the starboard wing under the pylon can containing the 2-DC instrument, and the data processing modules were mounted in a cabin rack. An IMU/differential GPS system is used to derive velocity and position relative to the ground, along with attitude (pitch, roll, and yaw) information. The AIMMS probe uses a five-hole hemispherical gust probe to derive air motion relative to the aircraft. The relative airflow parameters of true airspeed (TAS), angle of attack, and angle of side-slip are derived from pitot-static, vertical differential pressure, and horizontal differential pressure measurements on the hemispherical leading tip of the gust probe. Static pressure, air temperature, and relative humidity are also measured at the gust probe. Beswick (2008) provides an in depth description of the AIMMS probe.

Typically, the AIMMS probe is configured to output only processed data in real-time via a RS232 serial data feed. However, an additional processing module was added during the Spring 2009 Saudi Arabia project that recorded raw data to a USB drive at a frequency of 1 Hz. The raw data was post-processed using both Advantech's software and University of North Dakota (UND) developed software (Delene, 2011). The Advantech software used calibration parameters in configuration files to process the raw data files to create output files containing the wind parameters. The UND developed software, Airborne Data Processing and Analysis (ADPAA), is an open source software project (Source Forge, 2009). The ADPAA wind calibration and processing modules were developed for the UND's Citation Research Aircraft and were modified to create modules for use with the AIMMS probe. Since the ADPAA software is freely available, the source code can be independently varied. Having the code published enables researchers to know exactly what the code does and allows for outside scientists to continuously improve the code without the need for each research group to start from scratch.

2. Adventech's Calibration Method

a. Calibration Flight

While the pressure transducers used in the gust probe can be calibrated on the ground, an in-flight calibration is necessary to take into account installation and airflow effects. The airflow at the gust probe is deflected by the aircraft and nearby instruments, which causes the measured airflow angles at the probe to be different than the true airflow angles (airflow angles between aircraft axis and ambient airflow). Also, the probe experiences airflow deceleration due to air flowing around the wing, which affects the pitot-static and static pressure measurements and hence the TAS parameter (MacPherson and Baumgardner 1988). The AIMMS was calibrated on 21 March 2009 by performing maneuvers recommended by Advantech (personal communication with Bruce Woodcock). Yawing maneuvers (modulating heading via rudder while keeping wings level) and acceleration maneuvers were performed at two different airspeeds (80 and 120 m s^{-1}). The yawing maneuvers consisted of alternating rudder angle repeatedly so that aircraft heading was alternated approximately ±10 degrees from the desired heading. The yawing maneuver was performed at a true airspeed of 80 m s^{-1} and then again after increasing the true airspeed to 120 m s^{-1}. A reverse heading was flown and yawing maneuvers were again performed at 120 and 80 m s^{-1}.

The 21 March 2009 flight data was post processed using Aventech's software and calibration constants shown in Table 1 (personal communication with Bruce Woodcock). Both sets of calibration constants were similar, resulting in a similar wind solution. The calibration constants determined from the 21 March 2009 flight were used when computing the wind solution in this study.

These calibration constants are used to calculate angle of attack, angle of sideslip, and the static pressure error coefficient using the following equations

$$\alpha = a_0 + \left(\frac{P_U - P_L}{P_d - P_s}\right) a_\alpha + \left(\frac{P_r - P_l}{P_d - P_s}\right) a_\beta \tag{1}$$

$$\beta = b_0 + \left(\frac{P_U - P_L}{P_d - P_s}\right) b_\alpha + \left(\frac{P_r - P_l}{P_d - P_s}\right) b_\beta \tag{2}$$

$$C_p = c_0 + \left(\frac{P_U - P_L}{P_d - P_s}\right) c_\alpha + \left(\frac{P_r - P_l}{P_d - P_s}\right) c_\beta \tag{3}$$

respectively, where P_U, P_L, P_r, P_l, P_d, and P_s are the upper port pressure, lower port pressure, right port pressure, left port pressure, center pressure, and measured static pressure, respectively, $a_0, a_\alpha, a_\beta, b_0, b_\alpha, b_\beta, c_0, c_\alpha,$ and c_β are again calibration constants to be determined. $C_p = \frac{P_s - P_\infty}{\frac{1}{2}\rho_\infty {V_\infty}^2}$ where $\boldsymbol{C_p}$ is the static pressure error coefficient at the static pressure measurement location on the probe and P_∞, ρ_∞, and V_∞ are the pressure, density, and airspeed in the far field. Assuming inviscid and incompressible flow, $\frac{1}{2}\rho_\infty {V_\infty}^2 = P_d - P_s$. Multiplying the measured dynamic pressure ($P_d - P_s$) by the static pressure error coefficient, the static pressure position error can be found and applied to the measured static pressure. The measured dynamic pressure and calibrated static pressure along with temperature and humidity information can be used to calculate the true airspeed following Khelif 1999.

b. Validation Flight

Fig. 2 and Fig. 3, illustrates the maneuvers that were performed during the 23 March 2009 validation flight, which consisted of a straight and level flight leg at a constant airspeed for approximately three minutes, a series (3-4) of porpoise maneuvers (alternating elevator angle so that aircraft pitch alternated ± 5 to 10 degrees of the pitch required to hold altitude), and a series (3-4) of yawing maneuvers. After completing a single leg, the aircraft's heading was reversed and the sequence repeated in reverse order. A pair of legs was flown at 85, 105, and 130 m s^{-1} true airspeed at 4,572 m (15,000 ft) MSL, and then the complete sequence was performed again at 6,400 m (21,000 ft) MSL. These flight altitudes were chosen so the aircraft was in a uniform wind field well above the boundary layer. All time intervals used are included in the Appendix.

Fig. 4 shows box-and-whisker plots of the vertical wind during straight-and-level and porpoise maneuvers during the validation flight. At the 4,572 and 6,400 m MSL altitudes, the overall (all 12 legs) averaged median vertical wind was -23.1 ± 27.8 cm s^{-1} during the straight and level maneuvers, and -22.9 ± 34.8 cm s^{-1} during the porpoise maneuvers. The statistical distributions during pitching maneuvers have similar medians as the straight and level maneuvers but larger variations are observed, which indicates that not all of the aircraft motion has been removed during the maneuver.

Synoptic scale vertical motion in the mid-levels of the atmosphere is usually on the order of 1 cm s^{-1} (Bluestein 1992). Conventionally, the calibration constants used to convert vertical differential pressure into angle of attack are determined with the assumption that vertical wind is zero. Because vertical wind is assumed to be zero on the day of calibration when the wind could be non-zero, this non-zero wind can result in a slight offset in the vertical wind. The negative vertical velocities could be in part due to atmospheric vertical velocities being lower on the validation flight than the calibration flight, however, the observed difference of ~20 cm s^{-1} is likely not realistic since this value is an order of magnitude higher than typical synoptic scale vertical velocities.

3. University of North Dakota Calibration Method

a. Wind Equations

The University of North Dakota owns a Citation II Research Aircraft that has a nose boom with a 5-hole gust probe similar to the AIMMS Air Data probe. Ground relative parameters are provided by an Applanix airborne Position and Orientation system. Software written to calibrate the Citation Research Aircraft's wind system was modified to use measurements conducted on the 23 March 2009 flight to calibrate the AIMMS system. The basic form of the wind vector equation is given by Lenschow (1986) as

$$\boldsymbol{V} = \boldsymbol{V_a} + \boldsymbol{V_p} + \boldsymbol{\Omega X R} \tag{4}$$

where $\boldsymbol{V_a}$ is the velocity of the air relative to the aircraft, $\boldsymbol{V_p}$ is the velocity of the aircraft relative to the ground, $\boldsymbol{\Omega}$ is the three dimensional angular rotation rate of the aircraft, and $\boldsymbol{R}$ is the position vector of the gust probe relative to the IMU. The last term in Eq. 4 is takes into account the apparent velocities that would be observed by the gust probe due to the rotation of the aircraft when the gust probe is at some location away from the IMU. The vectors in Eq. 4 are all in the meteorological reference frame, where x is positive east, y positive north and z is positive upward and $\frac{dx}{dt} = u$, $\frac{dy}{dt} = v$, and $\frac{dz}{dt} = w$ are the three components of the wind velocity vector. The wind equations most often referenced were presented by Lenschow (1986) and are derived with the assumption that the gust probe is located along the longitudinal axis of the aircraft. The gust probe on the King Air was located on the wing, so the correct linear velocity term must be derived. The linear velocity term is found by first transforming $\boldsymbol{\Omega}$ and $\boldsymbol{R}$ from the aircraft reference frame to the local earth reference frame. In the aircraft reference frame, the x axis is the longitudinal aircraft axis positive off the nose, the y axis is the lateral aircraft axis positive in the starboard direction, and the z axis is the vertical aircraft axis positive downward (nadir). In the local earth reference frame, the x axis is positive north, the y axis is positive east, and the z axis is positive downward, which differs from the meteorological reference frame. The matrix to transform a vector from the aircraft reference frame to the local earth reference frame is given by Lenschow (1972) as:

$$[T] = \begin{bmatrix} cos\psi cos\Theta & -sin\psi cos\phi + cos\psi sin\Theta sin\phi & sin\psi \sin\phi + \cos\psi \sin\Theta \cos\phi \\ sin\psi cos\Theta & cos\psi cos\phi + sin\psi sin\Theta sin\phi & sin\psi sin\Theta cos\phi - cos\psi sin\phi \\ -sin\Theta & cos\Theta sin\phi & cos\Theta cos\phi \end{bmatrix}$$

where ψ, Θ, and ϕ are true heading, pitch, and roll angles respectively relative to the local earth reference frame. On the Research King Air, the distance of the gust probe along the x and z axis in the aircraft reference frame are considered negligible compared to the distance (5.918 m) along the y axis. The position vector of the gust probe in the local earth reference ($\boldsymbol{R_i}$) frame is then:

$$\boldsymbol{R_i} = [T] * \boldsymbol{R} = [T] * \begin{bmatrix} 0 \\ L \\ 0 \end{bmatrix} = L * \begin{bmatrix} -sin\psi cos\phi + cos\psi sin\Theta sin\phi \\ cos\psi cos\phi + sin\psi sin\Theta sin\phi \\ cos\Theta sin\phi \end{bmatrix}$$

where L is the distance between the gust probe and the aircraft's longitudinal axis. From Lenschow (1972), the angular rotation of the aircraft in the local earth reference frame is

$$\boldsymbol{\Omega}_i = \begin{bmatrix} -\dot{\Theta} sin\psi + \dot{\phi} cos\psi cos\Theta \\ \dot{\Theta} cos\psi + \dot{\phi} sin\psi cos\Theta \\ \dot{\psi} - \dot{\Theta} sin\Theta \end{bmatrix}$$

where $\dot{\psi}$, $\dot{\Theta}$, and $\dot{\phi}$ are derivatives with respect to time of heading, pitch, and roll respectively. The linear velocity term in the local earth reference frame then becomes:

$$\Omega_i X R_i = L *$$

$$\begin{bmatrix} \dot{\Theta}(cos\psi\, cos\Theta sin\phi + cos\psi sin\Theta cos\phi + sin\psi sin^2\Theta sin\phi) + \dot{\phi} sin\psi cos^2\Theta sin\phi - \dot{\psi}(cos\psi cos\phi + sin\psi sin\Theta sin\phi) \\ \dot{\Theta}(sin\psi cos\Theta sin\phi + sin\psi sin\Theta cos\phi - cos\psi sin^2\Theta sin\phi) - \dot{\phi} cos\psi cos^2\Theta sin\phi + \dot{\psi}(cos\psi sin\Theta sin\phi - sin\psi cos\phi) \\ \dot{\phi} cos\Theta cos\phi - \dot{\Theta} sin\Theta sin\phi \end{bmatrix}$$

To convert from the local earth reference frame to the meteorological reference frame, the relations $\psi = \psi_i - 90$, $u = -u_i$, and $w = -w_i$ are used. Applying these corrections and adding the linear velocity term to $\boldsymbol{V_p}$ and $\boldsymbol{V_a}$ terms given by Lenschow 1986, the full scalar wind equations used in this study are

$$u = u_p - u_a D^{-1}\Big(sin\psi cos\Theta + tan\beta(cos\psi cos\phi + sin\psi sin\Theta sin\phi) + tan\alpha(sin\psi sin\Theta cos\phi - cos\psi sin\phi)\Big) + L\left(\dot{\Theta}(sin\psi cos\Theta sin\phi + sin\psi sin\Theta cos\phi - cos\psi sin^2\Theta sin\phi) - \dot{\phi} cos\psi cos^2\Theta sin\phi - \dot{\psi}(sin\psi cos\phi - cos\psi sin\Theta sin\phi)\right), \quad (5)$$

$$v = v_p - u_a D^{-1}\Big(cos\psi cos\Theta - tan\beta(sin\psi cos\phi - cos\psi sin\Theta sin\phi) + tan\alpha(cos\psi sin\Theta cos\phi + sin\psi sin\phi)\Big) + L\left(\dot{\Theta}(cos\psi cos\Theta sin\phi + cos\psi sin\Theta cos\phi + sin\psi sin^2\Theta sin\phi) + \dot{\phi} sin\psi cos^2\Theta sin\phi - \dot{\psi}(\, sin\psi sin\Theta sin\phi + cos\psi cos\phi)\right) \quad (6)$$

$$\boldsymbol{w = w_p - u_a D^{-1}(sin\Theta - tan\beta cos\Theta sin\phi - tan\alpha cos\Theta cos\phi) + L(\dot{\Theta} sin\Theta sin\phi - \dot{\phi} cos\Theta cos\phi)} \quad (7)$$

where u_p, v_p, and w_p are the East, North, and upward components of aircraft velocity with respect to the ground respectively, u_a is the true airspeed, α and β are angle of attack and angle of sideslip respectively, and $D = (1 + tan^2\alpha + tan^2\beta)^{1/2}$.

b. Dynamic Pressure

The straight and level legs flown on 23 March 2009 were used to calibrate the dynamic pressure measurements from the gust probe on the Research King Air. The effect of airflow distortions induced by the aircraft on the measured dynamic pressure is taken into account by assuming the linear relation:

$$P_{ps} = I + S(P_d - P_s) \quad (8)$$

where I and S are the offset and sensitivity calibration constants, respectively. Because the wind is assumed to be constant well above the boundary layer, these calibration constants are determined by minimizing the difference in the mean wind vector between straight and level legs flown in reverse heading directions. True airspeed values from the ADPAA and Aventech software programs are shown in Fig. 5. Moist air thermodynamics were used in the calculation of true air speed (Khelif 1999).

c. Airflow Angle Calibration

The vertical and horizontal differential pressures were calibrated to obtain angle of attack (α), assuming the same linear relation as in the Aventech method (Eq. 1). The angle of attack calibration coefficients were determined using an iterative method that minimized the variance of the vertical wind and required that the overall mean vertical wind be as close to zero as possible during all porpoise maneuvers. Minimizing the variance of vertical wind stems from the assumption that for a large data set, values of calibration constants other than the correct values will result in an overall wind variance during the calibration maneuvers greater than the naturally occurring variance (Khelif, 1999).

Horizontal differential pressures were used to obtain angle of sideslip (β) assuming the same linear relation as the Aventech method (Eq. 2). The angle of sideslip calibration coefficients were determined by first calculating the mean horizontal components of wind without including angle of sideslip. The mean of each of the horizontal components of the wind calculated without angle of sideslip (μ_u and μ_v) are assumed to be equal to the mean horizontal components of the actual wind. The calibration constants in Eq. 2 are then found by minimizing the following expression for β variance:

$$\beta\, Var = (\mu_{u\beta} - \mu_u)^2 + s_{u\beta} + \left(\mu_{v\beta} - \mu_v\right)^2 + s_{v\beta} \tag{9}$$

where $\mu_{u\beta}$ and $\mu_{v\beta}$ are the mean east and north wind components calculated with angle of sideslip, μ_u and μ_v are the mean east and north wind components calculated without angle of sideslip, and $s_{u\beta}$ and $s_{v\beta}$ are the standard deviation of the east and north components of wind during the yawing maneuvers respectively. Minimizing the β variance in Eq. 9 allows calibration constants for Eq. 2 to be found that minimize the difference between the horizontal wind components derived with and without angle of attack and also minimize the variance in the horizontal components. Fig. 6 is an illustration of the results of this technique. The u component calculated assuming β = 0 has a significant dependence on angle of sideslip, while both the ADPAA and Aventech solutions show little dependence on angle of sideslip. Table 2 summarizes all the calibration constants determined from the 23 March 2009 validation flight for the ADPAA method.

4. Comparison and Discussion

The main difference between the ADPAA and Aventech calibration methods is how the dynamic pressure is calibrated. The ADPAA method assumes a simple linear relation between the calibrated dynamic pressure and the measured dynamic pressure (Eq. 8). The Aventech method assumes that the pitot pressure measured by the center port on the gust probe to be correct and instead calibrates the static pressure for a dependence on the airflow angles and dynamic pressure (Eq. 3). The differences between the resulting true airspeeds are shown in Fig. 5. The TAS solutions agree very well during the straight and level legs, but there are differences between the two solutions during the porpoise and sideslip maneuvers. During the porpoise maneuvers, the solution difference is greatest at the top and bottom of each porpoise, differing by approximately 1-2 m s^{-1}. Larger differences between the two solutions are seen during the sideslip maneuvers, where the solutions differ up to ~4 m s^{-1} when the aircraft is yawed to the left.

On a hemispherical gust probe, the center port on the gust probe is assumed to be at the actual stagnation point. When there is any angle between the airflow and the longitudinal axis of the probe, the measured pitot pressure would be less than the actual pitot pressure because the stagnation point is not directly over the center pressure port. Since the ADPAA method does not take airflow angles into account when calibrating the pitot-static pressure (dynamic pressure – static pressure), the TAS from the ADPAA solution is likely underestimated when large airflow angles exist. This error would increase with increasing airflow angles. The Aventech method calibrates the static pressure for airflow angles, resulting in higher airspeeds at higher airflow angles, which is shown during the porpoise and sideslip maneuvers in Fig. 7.

To see how the static pressure depends on airflow angles, the difference between the measured static pressure and the true static pressure in the far field at the same altitude was found. This difference in pressure is referred to as the static pressure defect. The static pressure far from the aircraft was approximated during sideslip and porpoise maneuvers assuming a hydrostatic atmosphere. Under the assumptions of a perfectly hydrostatic atmosphere with a lapse rate of 6.5 K/km and no aircraft effects on the measured static pressure, the static pressure defect should be zero. Any static pressure defect is due to aircraft’s influences on the static pressure measurement during the maneuver. Fig. 7 shows that the static pressure defect has a clear dependence upon angle of sideslip and TAS. Also, it appears that the static pressure defect on angle of sideslip at constant airspeed is not linear, with static pressure defect changing more with yawing to the left than to the right. Fig. 8 shows that the static pressure defect dependence on angle of attack has at least a loose linear relationship at a constant airspeed. The changes in

TAS during the porpoise maneuvers are only a result of exchanging kinetic energy for potential energy since the thrust is not altered. Because angle of attack is mostly a function of TAS, the porpoise maneuvers resulted in varying pitch more so than the angle of attack, which was only varied by 3^0 to 4^0 during the porpoise maneuvers. The angle of slideslip was varied by 20^0 during the sideslip maneuvers. Acceleration and deceleration maneuvers could be used to obtain a large continuous range of angle of attack. However, the since the static pressure depends on both the airspeed and angle of attack, the source of the static pressure defect would likely come partially from both parameters during porpoise maneuvers.

Box plots of each wind component from both solutions on 23 March 2009 are shown in Fig. 9. The ADPAA wind components were derived using the calibration constants determined on 23 March 2009, while the Aventech wind components were derived using the Aventech calibration performed on 21 March 2009. At 4,573 m (15000 ft), the Aventech horizontal wind components solution (Fig. 9, plots a and c) shows westerly winds with a magnitude of approximately 19 m s^{-1}. The first pair of reverse heading maneuvers shows significantly different values for both U (east/west) and V (north/sourth) wind components; however, there is no systematic bias in the wind components with aircraft heading. Furthermore, there is no systematic difference between the Aventech and ADPAA methods.

Table 3 gives vertical velocity summary statistics for all straight and level and porpoise maneuvers on the 23 March 2009 flight. The vertical velocity averages using the ADPAA method were much closer to zero than the Aventech method, however, this smaller difference is expected since the ADPAA calibration was performed using 23 March 2009 flight data whereas the Aventech solution used calibration constants determined on 21 March 2009. Synoptic scale vertical motion in the mid-levels of the atmosphere is usually on the order of 1 cm s^{-1} (Bluestein

1992); hence, the vertical wind derived using the Aventech method can be assumed to be an absolute vertical wind error. The 0.2 m s^{-1} absolute error from the Aventech method (**Error! Reference source not found.**) is similar to the 0.2-0.4 m s^{-1} vertical wind error on the Deutsches Zentrum fürLuft- und Raumfahrt (DLR) Falcon jet aircraft (Meischner et al., 2001).

The standard deviation differences in Table 3 and Table 4 are a measure of the variance introduced solely by aircraft maneuvers. Comparing the vertical wind from the Aventech and ADPAA methods, the standard deviation differences between the maneuver and the level legs from the Aventech solution were less than the ADPAA solution. The difference in the mean standard deviation differences (last column of Table 3) between each method was found to be significant at 4573 m (p value of 0.028), but not significant at 6400 m (p value of 0.475). The smaller differences in mean standard deviation between porpoise and level maneuvers indicate that the Aventech calibration method better corrects for the aircraft maneuvers in the W wind component solution compared to the ADPAA calibration method. The smaller standard deviation differences between porpoise and level maneuvers could be due to the fact the Aventech method takes into account the static pressure's dependence on airflow angles and airspeed. In the horizontal wind components, the mean standard deviations differences from the Aventech method were again smaller than the differences from the ADPAA solution at 4573 m, however, the difference between these differences in mean standard deviation (last column of Table 4) were not found to be statistically significant. The mean standard deviation differences from the Aventech solution were actually higher at 6,400 m. Both calibration methods do not completely remove the effects of aircraft maneuvers on the wind solution. It is difficult to discern whether one method handles the maneuvers better than the other method, however, the smaller mean standard deviation differences of the Aventech solution compared to the ADPAA solution at the lower altitude suggest the Aventech solution might handle the maneuvers better.

5. Conclusions

An Aventech AIMMS probe is useful in measuring the horizontal and vertical wind vector during airborne research projects. The true airspeeds from the Aventech and ADPAA methods agree very well when airflow angles are minimal and not varied, but diverge at high airflow angles. The static pressure measured under the wing is clearly dependent upon the airspeed and airflow angles. The static pressure calibration in the Aventech method takes airflow angles and airspeed into account, whereas the ADPAA method does not. The TAS determined from the Aventech solution is more realistic then the ADPAA solution and the ADPAA method should be modified to include a similar static pressure calibration.

The east wind components agree fairly well during the reverse heading maneuvers, while the smaller north components vary much more with reversing the heading (Fig. 9). The smaller north component during the reverse headings did not agree as well, with increasing differences in wind during reverse headings with increasing airspeed observed for measurements at 4,573 m and 6,400 m (not shown). The vertical wind standard deviation increases by less the 0.1 m/s during porpoise maneuvers for both the Aventech and ADPAA methods. Also, the increases in variance in the vertical wind due to aircraft maneuvers from the Aventech method were less than the ADPAA solution at both altitudes, and this difference was found to be statistically significantly less than the ADPAA at the lower altitude. The increases in variance from the Aventech method were less at 4,573 m and more at 6,400 m. No statistical significance was found when comparing the increases in variance due to maneuvers in the horizontal components. Neither method appears correct for maneuvers better in the horizontal components than the other.

Calibration and processing modules have been added into the open source ADPAA software package to enable the processing of raw data from the AIMMS probe. This enables further scientific research to be conducted with the AIMMS probe. Comparisons can be conducted between the AIMMS probe and other wind measurement system, such as UND Citation Research aircraft system, to directly compare measurement results. Such comparison could quantify the detailed error budgets for each system and clearly indicate where further improvements are possible. With the use of coupled GPS and INS systems (e.g. AIMMS), aircraft measured wind solutions accuracies have increased over older systems (Quante et al., 1996) that did not use GPS information; however, significant errors still remain and should be reduced to improve updraft velocity estimates for cloud microphysical research and the use of commercial aircraft based wind measurements in weather forecasting models (Moninger et al., 2010).

To improve the ADPAA method, a stagnation pressure measured by a pitot-tube with little dependence on airflow angles would be desirable over a dynamic pressure measured on a hemispherical gust probe, which would suffer from errors when high airflow angles exist. Also, the static pressure needs to be calibrated for airflow angles, which could be done by including terms that include dependence upon the vertical and horizontal differential pressures in the calibration model for static pressure. By removing the obvious dependence on airflow angles from the static and dynamic pressures, a more accurate true airspeed calculation can be made resulting in a more accurate wind solution.

6. ACKNOWLEDGEMENTS

Funding for this project was provided by the Presidency of Meteorology and Environment (PME), Kingdom of Saudi Arabia, through Weather Modification Inc. (WMI), of Fargo ND.

Weather Modification Inc. (WMI) instrumented and operated the Beech King Air 200 Research aircraft for the field project. We would like to thank all WMI pilots for safe and effective flying. WMI field technician, Todd Schulz and Albert (Swami) Kambli did an excellent job installing and maintaining the research instruments on the King Air 200 Research aircraft. University of North Dakota personnel, Gökhan Seven and Robert Mitchell, conducted instrument performance checks during field operations. The Saudi Arabia Presidency of Meteorology and the Environment staff provide weather forecast support during the field project.

7. Appendix

Table 5 includes all time intervals used for the analysis in this study.

8. REFERENCE

Axford, D. N., 1968: On the accuracy of wind measurements using an inertial platform in an aircraft, and an example of a measurement of the vertical mesostructure of the atmosphere. *J. Appl. Meteor.*, **7**, 645–666.

Bange, J., F. Beyrich, and D. A. M. Engelbart, 2002: Airborne measurements of turbulent fluxes during LITFASS-98: comparison with ground measurements and remote sensing in a case study. *Theor. Appl. Climatol.*, **73**, 35-51.

Beswick, K. M., M. W. Gallagher, A. R. Webb. E. G. Norton, and F. Perry, 2008: Application of the Aventech AIMMS20AQ airborne probe for turbulence measurements during the convective storm initiation project. *Atmos. Chem. Phys.*, **8**, 5449-5463.

Bluestein, H. B., 1992: Quasigeostrophic Theory. *Principles of Kenematics and Dynamics*, 1, *Synoptic-Dynamic Meteorology in Midlatitudes*, Oxford University Press, Inc, 300.

Crawford, T. L., and R. J. Dobosy, 1992: A sensitive fast-response probe to measure turbulence and heat flux from any airplane. *Boun.-Layer Meteor.*, **59**, 257-278.

Delene, D. J., 2011: Aircraft Data Processing and Analysis Software Package, *Earth Sci. Inform.*, **4**(1), 29-44, DOI: 10.1007/s12145-010-0061-4.

Delene, D. J., C. Grainger, P. Kucera, D. Langerud, M. Ham, R. Mitchell, and C. Kruse, The Second Polarimetric Cloud Analysis and Seeding Test, *J. Wea. Mod.*,43, 14-28, 2011.

Kalogiros, J. A. and Q. Wang, 2002: Calibration of a radome-differential GPS system on a twin otter research aircraft for turbulence measurements. *J. Atmos. Oceanic Technol.*, **19**, 159 –

171.

Karl, T., E. Apel, A. Hodzic, D. D. Riemer, D. R. Blake, and C. Wiedenmyer, 2009: Emissions of volatile organic compounds inferred from airborne flux measurements over a megacity. *Atmos. Chem. Phys.*, **9**, 271-285.

Khelif, D., S. P. Burns, and C. A. Friehe, 1999: Improved wind measurements on research aircraft. *J. Atmos. Oceanic Technol.*, **16**, 860–875.

Van Den Kroonenberg, A., T. Martin, M. Buschmann, J. Bange, and P. Vorsmann, 2008: Measuring the wind vector using the autonomous mini aerial vehicle M^2AV. *J. Atmos. Oceanic Technol.*, **25**, 1969 – 1982.

Kruse, C., Delene, D. J., Grainger, C, 2009: Evaluation of 3-dimensional winds measured by the Aircraft Integrated Meteorological Measurement System (AIMMS). Fall 2009 American Geophysical Union Conference. San Francisco, California.

Kucera, P.A., D. Axisa, R.P. Burger, D.R. Collins, R. Li, M. Chapman, R. Posada, T.W. Krauss, and A.S. Ghulam, 2010: Features of the Weather Modification Assessment Project in the Southwest Region of Saudi Arabia. *J. Wea. Mod*. Vol. 42, 63-88.

Lenschow, D. H., 1986: Aircraft measurements in the boundary layer. *Probing the Atmospheric Boun.-Layer Meteor.*, D. H. Lenschow, Amer. Meteor. Soc., 39–55.

Lenschow, D. H., 1979: Airborne measurements of the vertical flux of ozone ni the boundary layer. *Boun.-Layer Meteor.*, **19**, 249-265.

Lenschow, D. H., 1972: The Measurement of air velocity and temperature using the NCAR buffalo aircraft measuring system. NCAR-TN/EDD-74.

MacPherson, J. I., D. Baumgardner, 1988: Airflow about King Air wingtip-mounted cloud particle measurement probes. *J. Atmos. Oceanic Technol.*, **5**, 259-273.

Meischner, Peter, Robert Baumann, Hartmut Höller, Thomas Jank, 2001: Eddy Dissipation Rates in Thunderstorms Estimated by Doppler Radar in Relation to Aircraft In Situ Measurements. *J. Atmos. Oceanic Technol.*, **18**, 1609‑1627. doi: 10.1175/1520-0426(2001)018<1609:EDRITE>2.0.CO;2

Moninger, W., S. G. Benjamin, B. D. Jamison, T. W. Schlatter, T. L. Smith and E. Szoke 2010: Evaluation of Regional Aircraft Observations using TAMDAR, *Wea. Forecasting*, **25**, 627-645, 10.1175/2009WAF2222321.1.

Quante, M., P. R. A. Brown, R. Baumann, B. Guillemet, and P. Hignett, 1996: Three aircraft intercomparision of dynamical and thermodynamical measurements during the ‘Pre-EUCREX’ campaign. *Beitr. Phys. Atmos.*, **69**, 129‑146.

Saudi Arabia, 2009: http://aerosol.atmos.und.edu/UND_SaudiArabiaSpring2009_Report_100303.pdf, access 25, May 2011.

Snider, J. R., S. Guibert, J.-L. Brenguier, and J.-P. Putaud, 2003: Aerosol activation in marine stratocumulus clouds: Part 2. Köhler and parcel theory closure studies, J. Geophys. Res., 108(D15), 8629.

Source Forge, 2009: Airborne Data Processing and Analysis. http:// sourceforge.net/projects/adpaa/. Accessed July 2009.

Tjernstrom, M. and C. A. Friehe, 1991: Analysis of a radome air-mostion system on a twin-jet aircraft for boundary-layer research. *J. Atmos. Oceanic Technol.*, **8**, 19 – 40.

Wood, R., I. M. Stromberg, P. R. Jonas, and C. S. Mill, 1997: Analysis of an air motion system on a light aircraft for boundary layer research. *J. Atmos. Oceanic Technol.*, **14**, 960-968.

9. Figure Captions

Fig. 1: The Research King Air 200 aircraft with an Aircraft Integrated Meteorological Measurement System (AIMMS) installed. The AIMMS consists of a gust probe, a differential GPS, an inertial measurement unit (IMU), and a central processing unit (CPU). The IMU and CPU were mounted in the cabin, the gust probe was mounted under the right wing, and the GPS antennas were mounted on the top of each wing. The CPU processes data from the gust probe, GPS, and IMU to derive the wind velocity.

Fig. 2: Horizontal view illustrating the maneuvers conducted on a single leg of the 23 March 2009 validation flight.

Fig. 3: Plan view of the different legs flown on 23 March 2009 validation flight. The sequence was conducted at both 4,572 m (15,000 ft.) MSL and 6,400 m (21,000 ft) MSL.

Fig. 4: Box-and-whisker plot showing the distribution of 1 Hz vertical wind measurements during straight and level flight and pitching maneuvers at 4,572 m (15,000 ft., left) MSL and 6,400 m (21,000 ft. right) MSL. These wind measurements were produced using the Aventech calibration based on the 21 March flight. The star indicates the mean value, the horizontal line within the box is the median value, the top and bottom of the box is the 75^{th} and 25^{th} percentile respectively, and the top and bottom of the whiskers are the 95^{th} and 5^{th} percentiles respectively. Each pair of box-and-whiskers represents two maneuvers performed in opposite directions.

Fig. 5: Different solutions for True Air Speed (TAS) during straight and level, porpoise, and sideslip maneuvers on 23 March 2009. The Airborne Data Processing and Analysis (ADPAA) solution is represented by the line with plus signs, while the Aventech solution is represented by the solid black line.

Fig. 6: Illustration of angle of sideslip calibration during a yawing maneuver on the 23 March

2009 flight between 12:12:25 and 12:14:45 UTC. The east component of the wind calculated assuming $\beta = 0$ is represented by the solid black line, while the calibrated east component of wind from the ADPAA and Aventech solutions are represented by lines with plus signs and asterisks respectively.

Fig. 7: Static pressure defect found assuming a standard hydrostatic atmosphere during sideslip maneuvers between 12:08:24 and 12:50:10 UTC on 23 March 2009. The sideslip angles were found using the ADPAA calibration method. The colors indicate the True Airspeed (TAS) at which the measurement was made.

Fig. 8: Static pressure defect found assuming a standard hydrostatic atmosphere during porpoise maneuvers between 12:06:50 and 12:51:50 UTC on 23 March 2009. The sideslip angles were found using the ADPAA calibration method. The colors indicate the True Airspeed (TAS) at which the measurement was made.

Fig. 9: Box-and-whisker plots of the 1 Hz U (east/west), V (north/south), and W(up/down) wind components for 23 March 2009 at 4,573 m MSL using the Aventech and ADPAA methods (1^{st} and 2^{nd} columns respectively). The first six box-and-whisker plots in each plot were found during the straight and level legs, while the other six represent the measurements taken during the sideslip (U and V) and porpoise (W) maneuvers. The star indicates the mean value, the horizontal line within the box is the median value, the top and bottom of the box is the 75^{th} and 25^{th} percentile respectively, and the top and bottom of the whiskers are the 95^{th} and 5^{th} percentiles respectively. The heading direction is reversed between legs following the pattern described in Fig. 3.

10. Figures and Tables

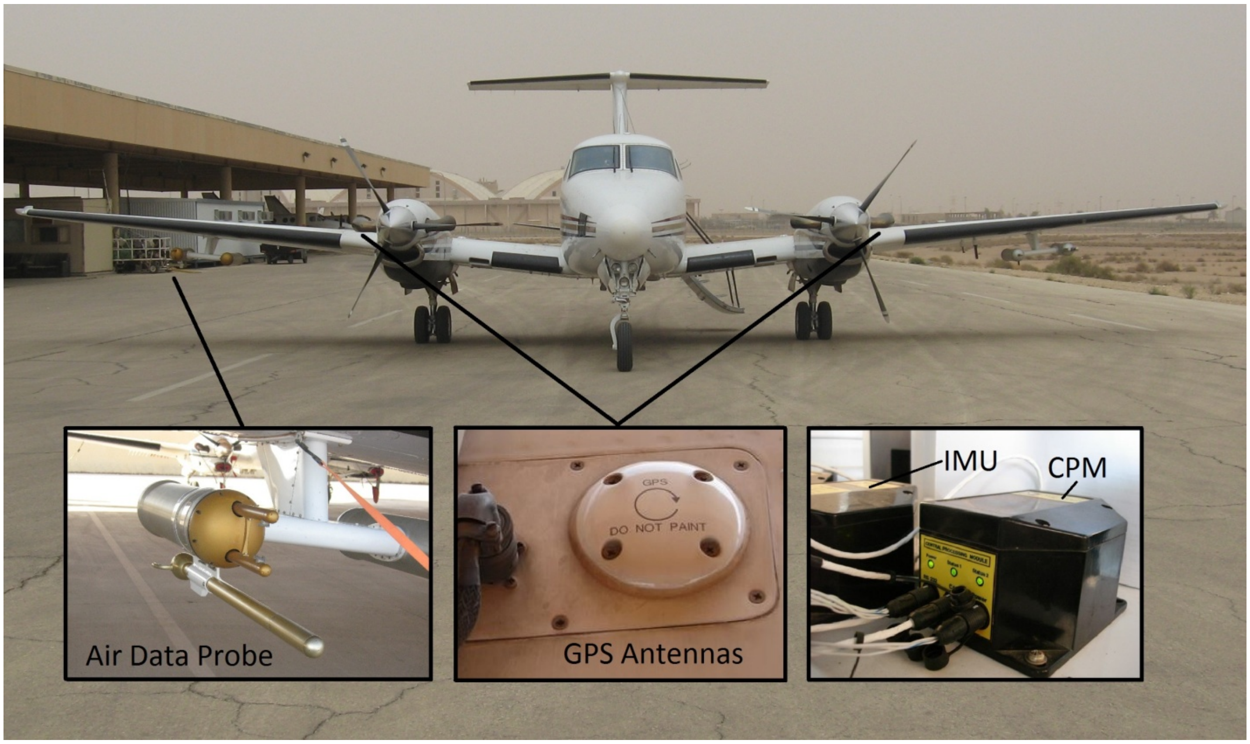

Fig. 1: The Research King Air 200 aircraft with an Aircraft Integrated Meteorological Measurement System (AIMMS) installed. The AIMMS consists of a gust probe, a differential GPS, an inertial measurement unit (IMU), and a central processing unit (CPU). The IMU and CPU were mounted in the cabin, the gust probe was mounted under the right wing, and the GPS antennas were mounted on the top of each wing. The CPU processes data from the gust probe, GPS, and IMU to derive the wind velocity.

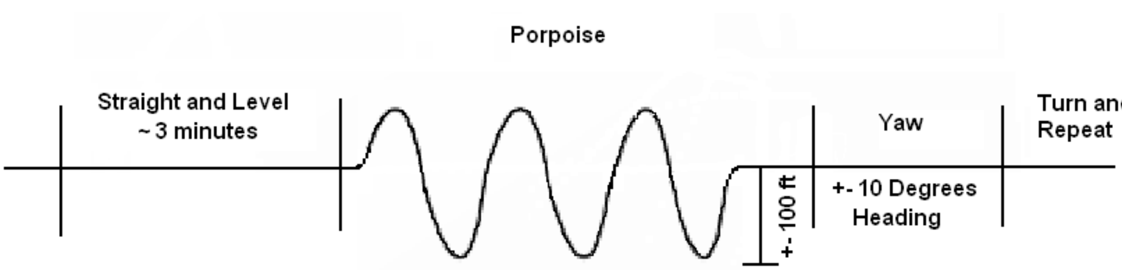

Fig. 2: Horizontal view illustrating the maneuvers conducted on a single leg of the 23 March 2009 validation flight.

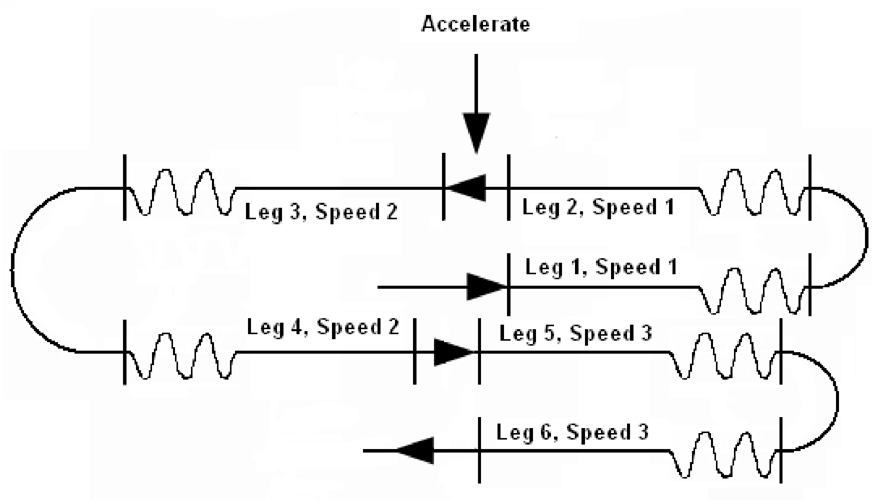

Fig. 3: Plan view of the different legs flown on 23 March 2009 validation flight. The sequence was conducted at both 4,572 m (15,000 ft.) MSL and 6,400 m (21,000 ft) MSL.

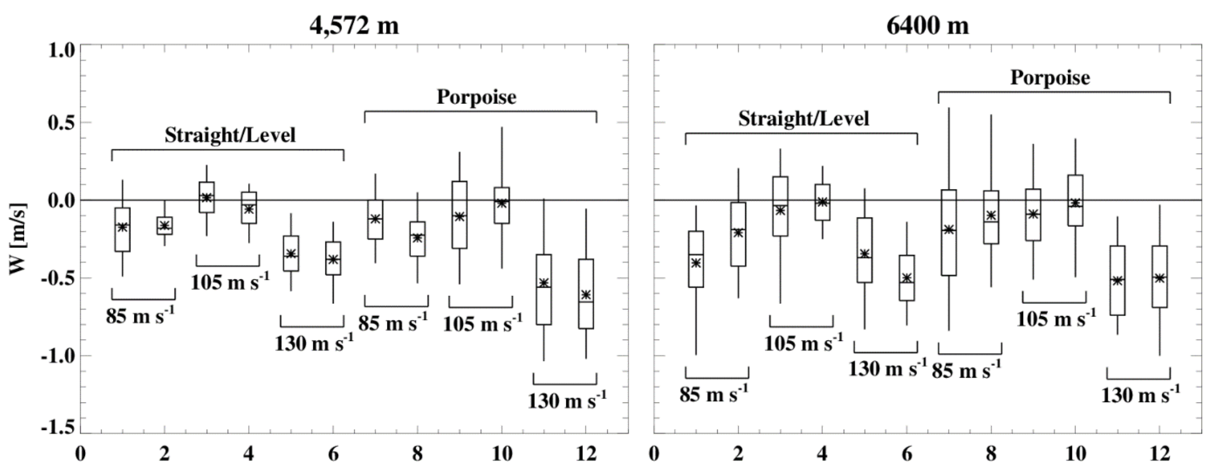

Fig. 4: Box-and-whisker plot showing the distribution of 1 Hz vertical wind measurements during straight and level flight and pitching maneuvers at 4,572 m (15,000 ft., left) MSL and 6,400 m (21,000 ft. right) MSL. These wind measurements were produced using the Aventech calibration based on the 21 March flight. The star indicates the mean value, the horizontal line

within the box is the median value, the top and bottom of the box is the 75th and 25th percentile respectively, and the top and bottom of the whiskers are the 95th and 5th percentiles respectively. Each pair of box-and-whiskers represents two maneuvers performed in opposite directions.

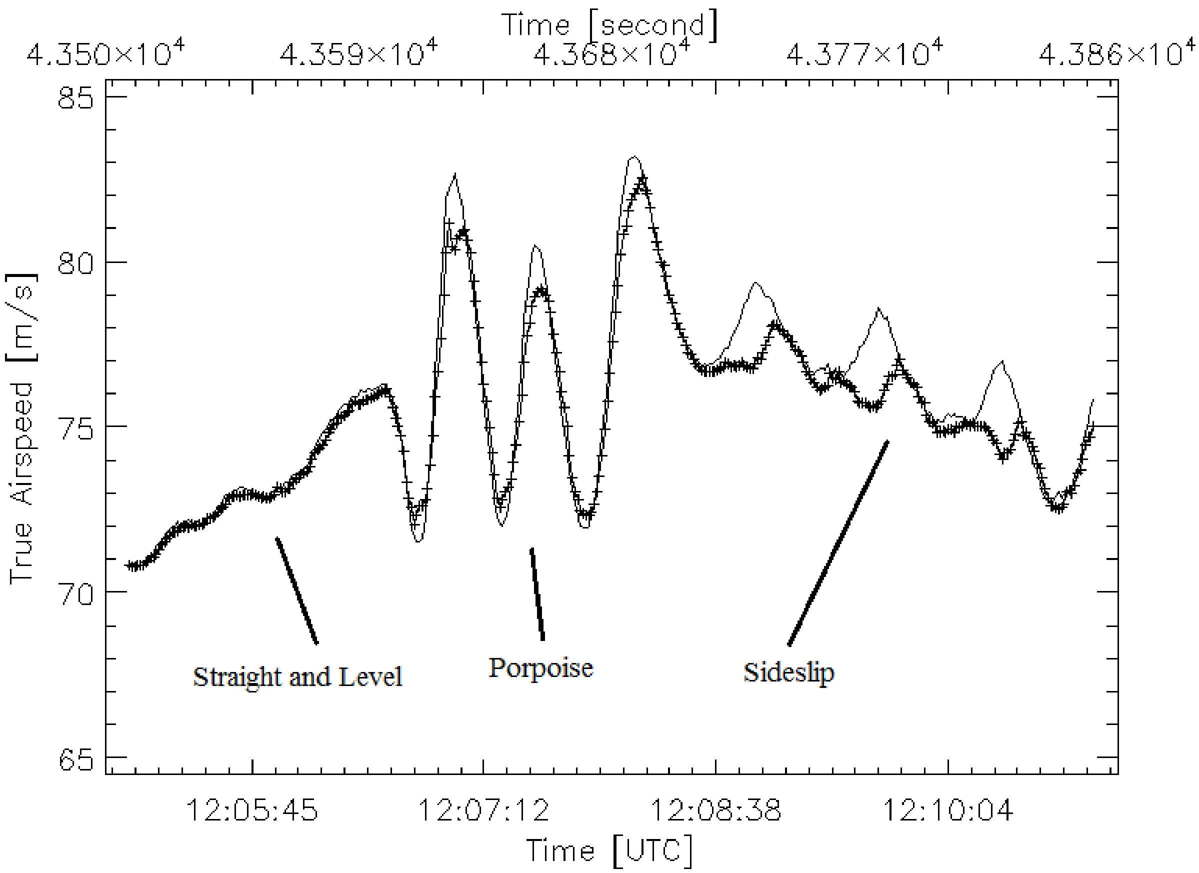

Fig. 5: Different solutions for True Air Speed (TAS) during straight and level, porpoise, and sideslip maneuvers on 23 March 2009. The Airborne Data Processing and Analysis (ADPAA) solution is represented by the line with plus signs, while the Aventech solution is represented by the solid black line.

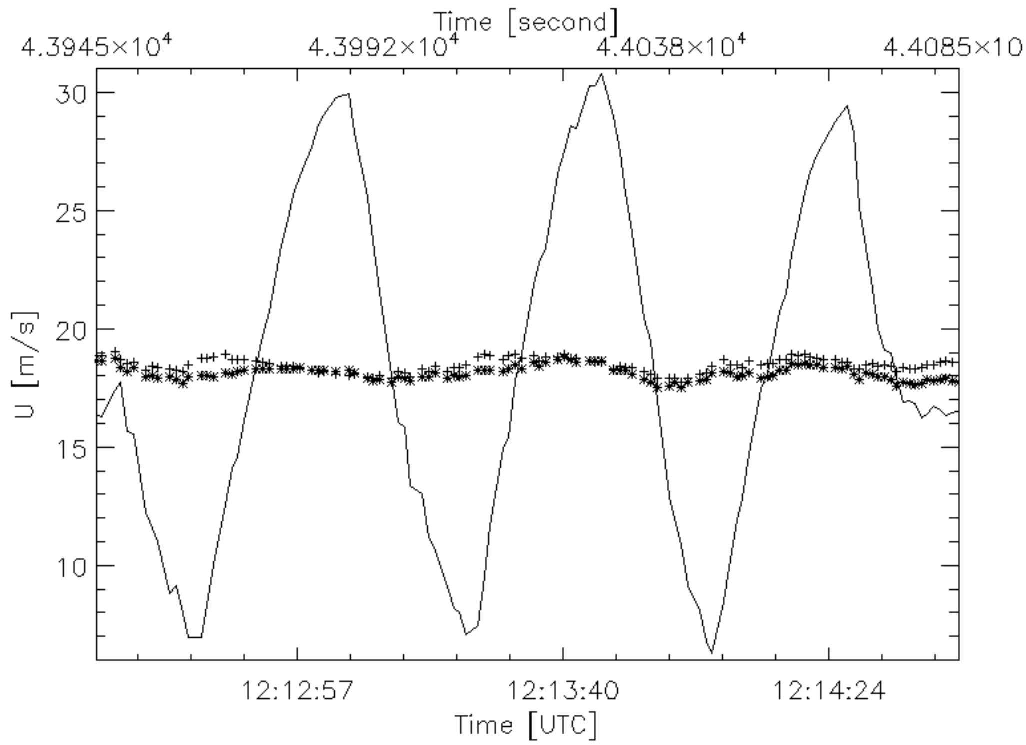

Fig. 6: Illustration of angle of sideslip calibration during a yawing maneuver on the 23 March 2009 flight between 12:12:25 and 12:14:45 UTC. The east component of the wind calculated assuming β = 0 is represented by the solid black line, while the calibrated east component of wind from the ADPAA and Aventech solutions are represented by lines with plus signs and asterisks respectively.

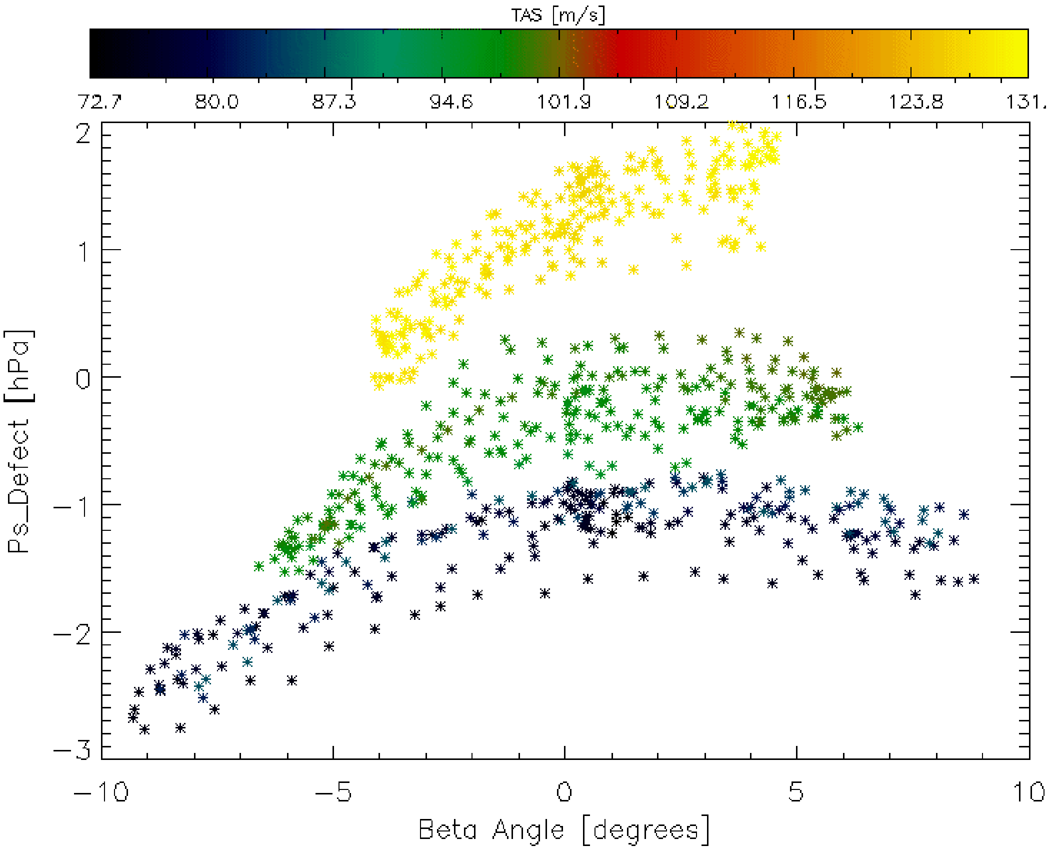

Fig. 7: Static pressure defect found assuming a standard hydrostatic atmosphere during sideslip maneuvers between 12:08:24 and 12:50:10 UTC on 23 March 2009. The sideslip angles were found using the ADPAA calibration method. The colors indicate the True Airspeed (TAS) at which the measurement was made.

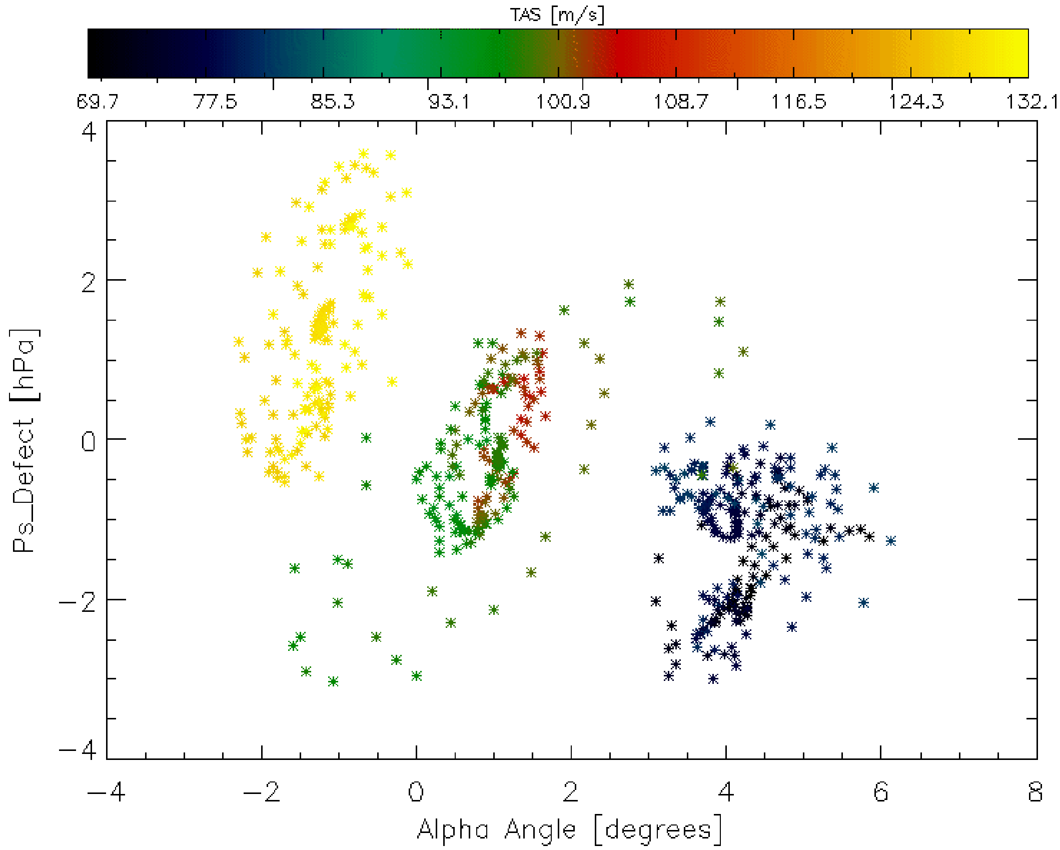

Fig. 8: Static pressure defect found assuming a standard hydrostatic atmosphere during porpoise maneuvers between 12:06:50 and 12:51:50 UTC on 23 March 2009. The sideslip angles were found using the ADPAA calibration method. The colors indicate the True Airspeed (TAS) at which the measurement was made.

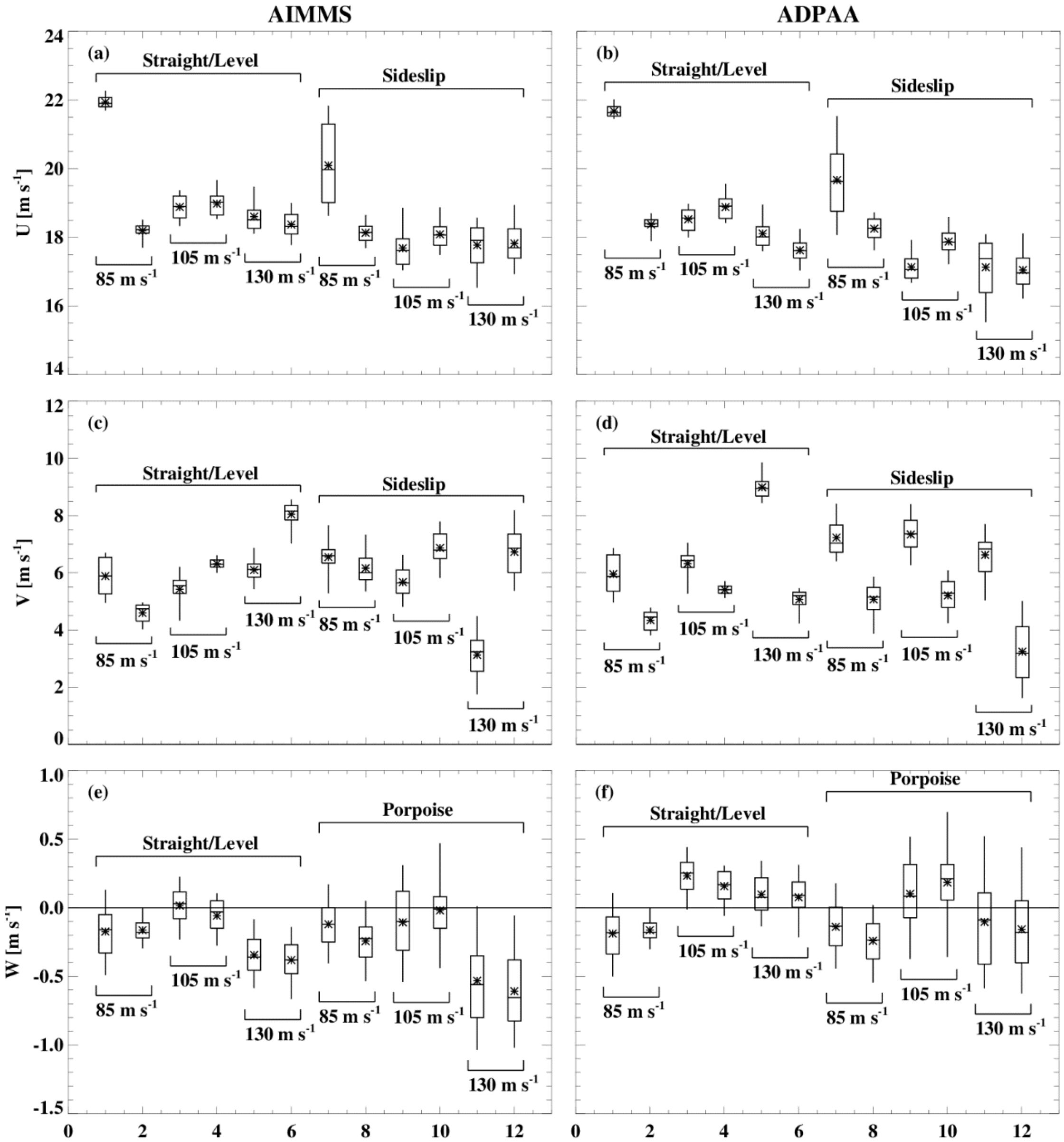

Fig. 9: Box-and-whisker plots of the 1 Hz U (east/west), V (north/south), and W(up/down) wind components for 23 March 2009 at 4,573 m MSL using the Aventech and ADPAA methods (1^{st} and 2^{nd} columns respectively). The first six box-and-whisker plots in each plot were found during the straight and level legs, while the other six represent the measurements taken during the sideslip (U and V) and porpoise (W) maneuvers. The star indicates the mean value, the horizontal line within the box is the median value, the top and bottom of the box is the 75^{th} and

25th percentile respectively, and the top and bottom of the whiskers are the 95th and 5th percentiles respectively. The heading direction is reversed between legs following the pattern described in Fig. 3.

Table 1: Summary of calibration constants from Aventech based on the flight data obtained on 21 March 2009 and 23 March 2009.

Parameter	a_0	a_α	a_β	b_0	b_α	b_β	c_0	c_α	c_β
21 March	0.525	7.569	-1.347	1.447	2.085	11.571	0.132	-0.0436	0.0463
23 March	0.537	7.514	-1.199	0.078	2.070	11.537	0.133	-0.0445	0.0680

Table 2: Summary of calibration constants determined using the ADPAA method to calibrate the AIMMS based on the flight data obtained on 23 March 2009.

Parameter	S	I	α_0	α_α	α_β	β_0	β_α	β_β
Value	1.0391	2.6960	0.3576	7.3165	-1.2519	1.4694	1.8578	11.6580

Table 3: Summary statistics of vertical velocity during all (both altitudes) straight and level and porpoise maneuver legs on 23 March 2009 for the ADPAA and Aventech methods. The mean and standard deviations (STDEV) were computed from all 1 Hz measurements during each leg. The mean STDEV was calculated by averaging the 12 standard deviations calculated for each time interval leg.

Method	Altitude	Average during Legs [m s^{-1}]		Average of the Legs STDEV [m s^{-1}]		STDEV Difference [m s^{-1}]
		Porpoise	Level	Porpoise	Level	Porpoise-Level
Aventech	4,573 m	-0.246±0.328	-0.187±0.208	0.259±0.060	0.143±0.034	0.116
	6,400 m	-0.208±0.369	-0.239±0.311	0.306±0.067	0.252±0.055	0.054
ADPAA	4,573 m	-0.063±0.312	0.042±0.214	0.279±0.070	0.140±0.033	0.138
	6,400 m	0.027±0.345	0.058±0.304	0.311±0.053	0.248±0.055	0.063

Table 4: Summary statistics of the horizontal wind for all straight and level and sideslip maneuver legs on 23 March 2009 for the ADPAA and Aventech methods. The mean and standard deviations (STDEV) were computed from all 1 Hz measurements during each leg. The mean STDEV was calculated by averaging the standard deviation calculated for each time interval leg.

Method	Altitude [m]	Component	Average during Legs [m s^{-1}]		Average of the Legs STDEV [m s^{-1}]		STDEV Difference [m s^{-1}]
			Sideslip	Straight	Sideslip	Straight	Porpoise-Straight
Aventech	4573	U	18.271±1.055	19.209±1.338	0.601±0.283	0.318±0.096	0.283
		V	5.932±1.387	6.103±1.120	0.682±0.134	0.416±0.159	0.266
ADPAA		U	17.856±1.148	18.889±1.393	0.610±0.304	0.311±0.096	0.299
		V	5.772±1.660	6.138±1.556	0.731±0.178	0.408±0.163	0.323
Aventech	6400	U	28.777±1.381	31.325±1.781	1.062±0.348	0.997±0.310	0.065
		V	0.065±1.531	-0.740±0.881	0.802±0.100	0.478±0.113	0.325
ADPAA		U	28.172±1.348	30.769±1.657	1.027±0.377	0.984±0.296	0.047
		V	0.101±1.634	-0.913±1.912	0.729±0.179	0.487±0.131	0.242

Table 5: Time (UTC) intervals of each maneuver preformed on 23 March 2009.

Straight and Level		Porpoise		Sideslip	
Start	End	Start	End	Start	End
12:03:26	12:06:36	12:06:50	12:08:40	12:08:24	12:10:34
12:16:53	12:19:19	12:14:50	12:16:38	12:12:25	12:14:46
12:22:07	12:25:21	12:26:00	12:28:00	12:28:07	12:30:17
12:35:06	12:37:48	12:34:10	12:36:20	12:31:48	12:33:45
12:39:57	13:43:16	12:43:30	12:44:35	12:44:40	12:46:26
12:51:26	12:54:29	12:50:30	12:51:50	12:47:59	12:50:10
13:01:40	13:03:08	13:03:30	13:05:04	13:04:42	13:06:09
13:10:11	13:12:00	13:09:05	13:10:40	13:07:15	13:08:54
13:18:11	13:21:14	13:21:30	13:22:55	13:22:48	13:24:17
13:28:20	13:31:48	13:27:10	13:28:55	13:25:26	13:26:55
13:36:36	13:39:27	13:39:50	13:40:50	13:40:43	13:42:35
13:47:59	13:51:14	13:47:05	13:48:25	13:45:11	13:46:47